www.czasopisma.pan.pl PAN POLSKA AKADEMIA NAUK www.journals.pan.pl

PAN ARCHIVES OF ACOUSTICS
Vol. **37**, No. 3, pp. 253–260 (2012)

DOI: 10.2478/v10168-012-0033-4

Multimodal Ultrasonic Imaging for Breast Cancer Detection

Jorge CAMACHO, Luis MEDINA, Jorge F. CRUZA, José M. MORENO, Carlos FRITSCH

Ultrasound for Medical and Industrial Applications Group (UMEDIA)
Spanish National Research Council (CSIC)
La Poveda (Arganda), 28500 Madrid, Spain; e-mail: j.camacho@csic.es

(*received January 20, 2012; accepted May 15, 2012*)

Ultrasound is used for breast cancer detection as a technique complementary to mammography, the standard screening method. Current practice is based on reflectivity images obtained with conventional instruments by an operator who positions the ultrasonic transducer by hand over the patient's body. It is a non-ionizing radiation, pain-free and not expensive technique that provides a higher contrast than mammography to discriminate among fluid-filled cysts and solid masses, especially for dense breast tissue. However, results are quite dependent on the operator's skills, images are difficult to reproduce, and state-of-the-art instruments have a limited resolution and contrast to show micro-calcifications and to discriminate between lesions and the surrounding tissue. In spite of their advantages, these factors have precluded the use of ultrasound for screening.

This work approaches the ultrasound-based early detection of breast cancer with a different concept. A ring array with many elements to cover 360° around a hanging breast allows obtaining repeatable and operator-independent coronal slice images. Such an arrangement is well suited for multi-modal imaging that includes reflectivity, compounded, tomography, and phase coherence images for increased specificity in breast cancer detection. Preliminary work carried out with a mechanical emulation of the ring array and a standard breast phantom shows a high resolution and contrast, with an artifact-free capability provided by phase coherence processing.

Keywords: ultrasound imaging, ultrasound tomography, breast cancer.

1. Introduction

Ultrasonic imaging is a common practice for medical diagnosis in many specialties from more than three decades. For early breast cancer detection, it is a technique that currently complements the information provided by a previous mammography, the standard screening technique. The aim of screening is detection of small and pre-invasive tumors in asymptomatic women to achieve a high rate of treatment success. However, since mammography measures tissue density, it produces a high level of false negatives in women with dense breasts and, since it uses ionizing radiation, the interval between examinations must be no less than one year, giving rise to the so-called interval cancer (Berry *et al.*, 2005).

Current ultrasound practice is based on echography, where the operator positions by hand the transducer over the patient's body. Ultrasound has many advantages over other imaging techniques like X-rays, TAC, MRI, PET, etc. because it uses non-ionizing radiation, provides high-contrast real-time images, equipment is less expensive, and its application is pain-free. Furthermore, with regard to mammography, ultrasound images allow a cleaner distinction between fluid-filled cysts and solid masses. But, in spite of their advantages, current ultrasound technology and procedures have limitations that, following international guidelines, have precluded its use as a screening tool for breast cancer. The main reasons are the sensitivity dependence on the operator skills, the difficulty for imaging and registering the whole breast, and the lack of resolution to detect micro-calcifications (Teh, Wilson, 1998).

The first two limitations are due to the operational procedure. Images are taken by hand from different orientations, which makes it difficult to obtain repeatable results in a historical perspective. Also, the detection and location of a tumor greatly depends on the operator's experience. Moreover, reflectivity ultrasound images display differences in the acoustic impedance of tissues, which may be subtle, with low specificity

for tumor distinction from the surrounding healthy tissue. This way, ultrasound is just used as a complementary technique to mammography (Nothacker *et al.*, 2009).

However, some recent developments try to overcome these limitations with automatic imaging systems based on ring transducers with a large amount of elements. The ring array surrounds a hanging breast immersed in a water-bath (Stozka *et al.*, 2004; Waag *et al.*, 2006; Duric *et al.*, 2007). With this circular geometry, slice images at coronal planes are acquired. Moving the ring array vertically one can obtain a volumetric image (Fig. 1a). This arrangement avoids the problems associated with scanning the transducer by hand, so that the images are repeatable. The circular geometry provides an increased resolution which may be determined by the signal bandwidth instead of the aperture size. This is useful to improve the detection of micro-calcifications.

a)

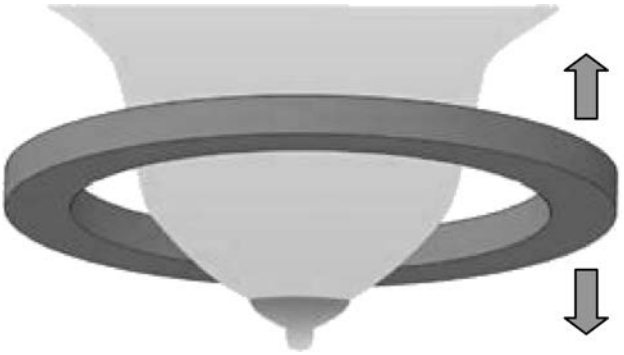

b)

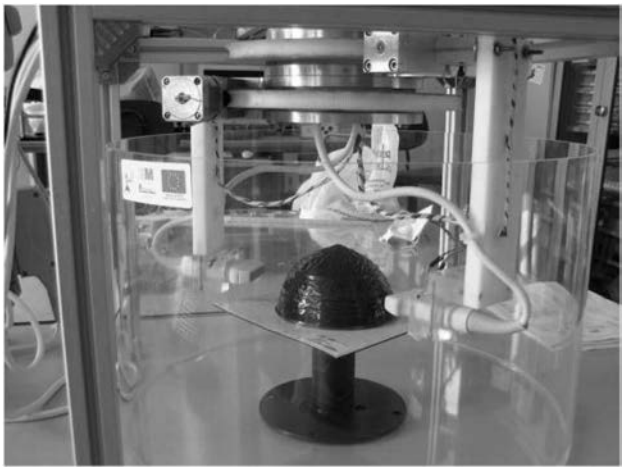

Fig. 1. a) Concept for breast imaging in real-time based on a circular array with thousands of elements, b) experimental arrangement with mechanically rotated conventional arrays.

On the other hand, other imaging modalities may provide increased specificity for breast cancer detection, as it has been shown with ultrasound velocity transmission tomography (Li *et al.*, 2008). One of its advantages is that it provides quantitative data of the whole breast, and transmission measurements are independent of echo images.

A recent achievement of our group provides an improved resolution and contrast for ultrasonic images by means of *phase coherence processing* (Camacho *et al.*, 2009). Furthermore, this technique complements the others by suppressing grating lobes, sidelobes, and reverberation artifacts.

This work presents a low-cost arrangement to experiment with different imaging modalities. A standard breast-mimic phantom that includes low and high scatterer density cysts and micro-calcifications is used for imaging. To avoid the expenses of a ring array with thousands of elements standard 128-element arrays have been used for this preliminary study. The arrays are mechanically rotated to emulate a circular aperture (Fig. 1b). Commercial equipment with pulse-echo and transmission capability is used for the experiments. This arrangement allows easy testing of different ultrasound imaging modalities at the expense of a rather large acquisition time.

2. Imaging modalities with circular arrays

Conventional echography uses linear or slightly curved arrays of N independent transducer elements. Beam steering and focusing is carried out by electronic means, using a set of fixed delays for the individual excitations and dynamically changing the delays for the signals received by every element. This is the standard *phased array* technique that provides images in real time and, in practice, the only ultrasonic imaging modality used for diagnostic purposes. However, with a circular array surrounding the inspected body, several other modalities are possible, in particular: *synthetic aperture*, *transmission tomography*, and *phase coherence imaging*. All these methods, described in this section, are being implemented in the present system and are the basis of our multi-modal approach. Finally, in section 5, first results with *phased array image compounding* and *phase coherence imaging* are presented.

2.1. Phased array and image compounding

Phased array image quality is limited by several factors. First, while dynamic focusing is applied in reception, focusing in emission is performed at a single depth to keep a relatively high frame rate. Thus, resolution is better at the focus proximities.

Second, the lateral resolution Δx improves with the aperture size D:

$$\Delta x = k\frac{\lambda}{D}z, \tag{1}$$

where k is a constant (≈ 1), λ is the wavelength, and z is depth. Therefore, the larger the aperture, the better the resolution. But, to avoid grating lobe artifacts,

the distance d between elements must be kept below $\lambda/2$, so that a high number N of elements and associated electronic channels is required to obtain a large aperture $D = N \cdot d$.

Third, the sidelobes level limits the contrast and dynamic range of phased-array images. Apodization techniques help to reduce their impact at the expense of some losses in the lateral resolution (Szabo, 2004). On the other hand, a single phased array image composed of L scan-lines over a length z can be acquired and processed in a time,

$$T_P = \frac{2z}{c} L. \tag{2}$$

For $z = 150$ mm, $c = 1.5$ mm/μs, and $L = 150$, the acquisition time is $T_P = 30$ ms and the frame rate that can be reached is 33 images/s (real-time imaging).

The phased array technique can be advantageously used in a circular geometry. A large set of sector images with active apertures at different angular positions can be averaged in the overlapping region to form the final image (Fig. 2). This process is known as *image compounding* and has been previously used with conventional arrays, getting contrast improvements and clutter reductions (Jespersen *et al.*, 1998).

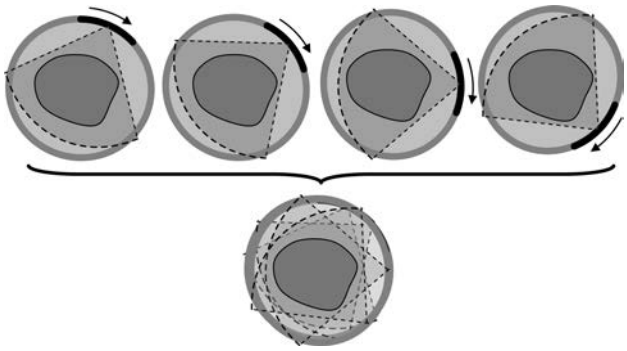

Fig. 2. Compound image built from sector phased array images with a circular array geometry.

A time $T_C = n \cdot T_P$ is required to acquire a single compound slice image built from $n$phased array images taken at $360°/n$ angular intervals. This takes about 0.5 s per slice image with the above parameters and $n = 16$. By vertically moving the ring array a set of 120 slices can be obtained in 60 seconds, which is a rather high time interval for the clinical use. However, since the results are obtained in real-time, the operator can set the vertical position of the ring array for zooming and looking for details. This is useful for *in-situ* diagnostics and deciding whether further explorations or proofs are necessary.

2.2. Synthetic aperture techniques

Another approach is based on *synthetic apertures*. The "gold standard" is *the synthetic transmit aperture* or STA. A single or a reduced set of elements generate an omnidirectional wavefront. The whole N-elements aperture is used in reception, and a *low-resolution image* is obtained by compensating the time-of-flight differences from the emitter to every imaged point and back to each receiver element. This process is repeated N times, changing the position of the emitter. Adding together the low-resolution images yields an image focused in emission and reception with a high resolution and contrast (Trots *et al.*, 2010). The cost of this technique is the huge data volume generated and the requirements for a high performance hardware. The current technology does not allow obtaining the STA gold standard in real time (Jensen *et al.*, 2005).

Various approaches that are based on the effective aperture concept allow reducing the number of emissions, so that the frame rate can be increased with regard to the phased array technique, while preserving a high resolution and dynamic range, at the cost of a reduced signal-to-noise ratio (Nikolov, Behar, 2005). Some of these alternatives also reduce the number of receiving elements, which achieves real-time imaging with the use of GPUs (Romero *et al.*, 2009).

Synthetic aperture techniques can also be applied in a circular geometry (Fig. 3) with further resolution improvements. The combined effect around 360° approaches the radial resolution Δz of every partial image. In fact, given by the transducer bandwidth B:

$$\Delta z \approx \frac{c}{2B} \approx \lambda. \tag{3}$$

Differently from (1), this equation yields a depth-independent resolution. Moreover, for $z{>}D$ (that is, $F\# > 1$), Eq. (3) yields a better resolution than (1). To this purpose, the image is progressively formed in a rectangular grid using the analytic signal to preserve the phase information, so that constructive and destructive interferences take place at building the final image.

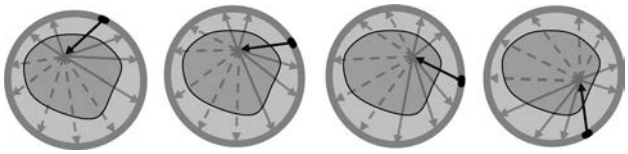

Fig. 3. STA imaging: a small aperture is used for omnidirectional emission and a large one for reception. The analytical signal corresponding to the time-of-flight from the emitter to every image pixel and to every receiving element is obtained. Then, the emitter aperture is moved by an angular interval and the process repeated. The final image results by averaging all the partial images.

The acquisition time for every low-resolution image is,

$$T_S = \frac{2z}{c}. \tag{4}$$

With the parameters given, each low-resolution image is acquired in 0.2 ms. Taking these images at 0.5° intervals around the circle, the acquisition time for a slice is 144 ms (composition of 720 low-resolution images). To get the full volume of 120 slices, a total time lower than 18 seconds is required. This is a good figure for the clinical use.

However, there are also other associated costs. The computing time and data volume have not been considered in the previous calculation. In a circular image of a 150 mm diameter with the resolution of 0.1 mm there are about 1.8 Mpixels. Using receiving apertures of $N = 256$ elements, every partial image requires processing 460 MS (complex samples) with the delay-and-sum algorithm. A slice composed from 720 low-resolution images requires processing of around 330 GS, and the whole volumetric image amounts for 40 TS. Processing and storing this huge information volume can take much longer than the acquisition time, even if a specialized hardware is used to accelerate the process.

On the other hand, at 0.5° intervals in a ring transducer of a 100 mm radius, the distance between emitters is about 0.9 mm, which represents 6λ for a 5 MHz frequency transducer. As the inter-element distance must be kept below $\lambda/2$ to avoid grating lobes, the number of array elements should be $N \approx 4200$. As a solution of this problem, techniques based on the effective aperture concept could be explored to obtain an equivalent dense circular aperture with fewer electronic channels but the same high number of array elements.

Phase coherence processing which suppresses grating lobes, as it is explained below, may be a better alternative. If the inter-element pitch is increased from $\lambda/2$ to approximately 2λ, the number of elements and associated electronic channels is reduced by four (for example, to 1024 channels). This is beneficial to lower the implementation costs, as well as to reduce the data volume involved in the acquisitions.

2.3. Transmission tomography

Finally, the third imaging modality is transmission *tomography*. In this case, two opposing apertures are used in a through-transmission mode, one acting as the emitter and the other as receiver (Fig. 4). The emitter is created by a reduced set of array elements to produce a fan-beam illuminating the inspected body. The time-of-flight from emission to reception is recorded at every element of the opposite receiving aperture. This is repeated many times changing the angular position to cover the 360° circumference, keeping both apertures in opposite sides.

Computed tomography algorithms, modified to take into account ultrasound refraction with changes in the propagation velocity, are applied to obtain velocity images (Quan, Huang, 2007).

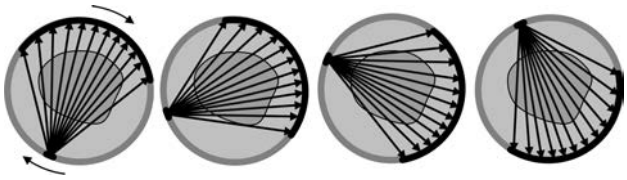

Fig. 4. Ultrasound transmission tomography arrangement with fan-beams.

Basically, for straight-ray paths, a rectangular grid is defined with M cells small enough to consider constant the propagation velocity within the cell. If the total number of rays generated around the circle is N, the time-of-flight of the ray i is,

$$T_i = \sum_{j=1}^{M} l_{ij} b_j, \tag{5}$$

where b_j is the inverse of the sound velocity at cell j (*slowness*), and l_{ij} is the length of the ray i when crossing the cell j, which is frequently set to one if the ray crosses the cell or to zero if it does not. This is a system of N equations with M unknowns $\{b_j\}$, where usually $N > M$, that can be solved by the least squares method. Numerical techniques to avoid the ill-conditioned equations (the values of T_i are large and those of l_{ij} are small) must be applied and a subset of equations can be used (Duric *et al.*, 2005). In order to take into account the ray bending due to refraction, an iterative procedure is followed, progressively refining the slowness values found for every cell (Li *et al.*, 2008).

Acquisition time for ultrasound tomography depends only on the number of emissions if parallel receiving channels are available. For 360° emissions (at intervals of 1°) with a ring array of 200 mm diameter, a single slice can be acquired in less than 60 ms. This way, the volumetric data of 120 slices would take about 7 seconds, which is a very good figure for the clinical use.

2.4. Phase coherence imaging

Phase coherence imaging (PCI) yields an image of the phase concentration of the received signals after application of the focusing delays (*aperture data*). PCI can be used with the phased array, as well as with the synthetic aperture modalities by providing, at every pixel, a coherence factor with values in the range [0, 1] (Camacho *et al.*, 2009).

Basically, it measures the focus quality so that, when the received signals originated at the focus, the coherence factor approaches unity, while for the out-of focus signals it tends to zero. This way PCI is insensitive to side and grating lobes, as well as to reverberations, since these indications are produced in regions far away from the focus. By the way, this reduces the main-lobe width, which also improves resolution.

PCI image itself is useful to show weak reflectors immersed in clutter (like micro-calcifications), since the coherence factor does not depend on the reflected signal amplitudes and, the clutter, originated by unresolved scatterers in the range cell, is simultaneously reduced. Besides, PCI improves the resolution and contrast of the phased array and synthetic aperture images by weighting the output of these beamformers.

Its operation does not require additional acquisition time when jointly used with the phased array or with synthetic aperture techniques, since a specific hardware can obtain the coherence factors in real-time.

3. Experimental arrangement

A first experimental arrangement is presented in Fig. 1b, where a cylindrical tank, two independent arms holding linear 128-element arrays of 5 MHz (Prosonic, Korea) and a breast phantom (Gammex-RMI, USA) are shown. Independent circular movement is provided by means of worm and wheel attachments driven by stepper motors that offer a high mechanical resolution (0.1°) and low hysteresis. The motors were individually controlled by our own designed drivers with the USB interface. Both array arms can be independently and freely moved with the limitation that their relative angular distance cannot be less than 30° because they lie in the same plane. Figure 5 shows a schematic representation.

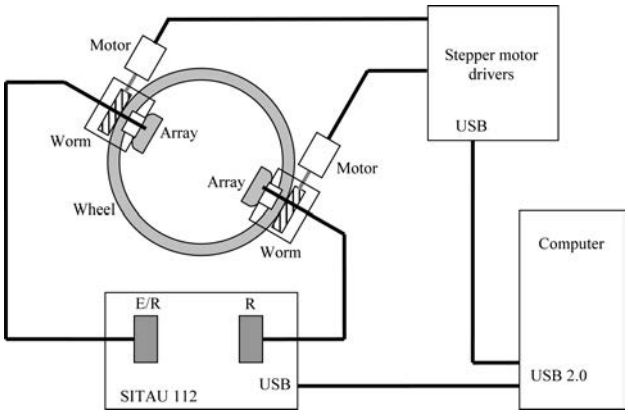

Fig. 5. Schematic representation of the experimental arrangement.

A phased array SITAU 112 system (Dasel, Spain), with 128 pulse-echo and transmission channels in parallel, was used to acquire and process the ultrasonic data. This instrument is connected to a computer by means of an USB-2.0 interface. The computer receives and further processes data provided by the ultrasonic equipment with programs written in MATLAB (The Mathworks, USA) that also control motor movements.

This arrangement can be used to emulate a ring array composed of thousands of elements at low-cost, but without high frame-rate capabilities. However, since the arrays are linear, the emulated geometry is not circular but polygonal. This has little importance as long as the accurate position of every element is known. This requires a calibration procedure that, anyway, must be also followed for circular arrays to compensate for possible manufacturing gaps and tolerances. Furthermore, a polygonal ring composed of independent linear arrays may be less expensive than a single circular array. Also, such an arrangement is easier and cheaper to maintain if dead elements appear by simple substitution of the damaged array.

4. Calibration procedure

Precise knowledge of all operating parameters is essential to obtain high quality images. In particular, the sound velocity in the coupling medium (water) must be accurately evaluated, as well as the positions of all the array elements with regard to a reference coordinate system. Since the mechanics is precise, circular movement can be assumed, although with an unknown radius.

The calibration takes place in two steps. First, the sound velocity is evaluated using a phantom composed of two parallel 0.1 mm diameter copper wires ($\lambda/3$ at 5 MHz). The distance between the wires is accurately known and a base plate assures their vertical position. This phantom is set alone in an arbitrary position of the tank filled with water.

Using a single element of an array in pulse-echo, a search is performed to find the angular position where the time interval between both wire echoes is at maximum. In this situation the element and wires are aligned, and the sound velocity is obtained as double the wire distance divided by the time interval among echoes.

The second step determines the element positions. To this purpose, it is enough to find the radius R to the array center and the angle β formed by the radius and the normal to the array (Fig. 6). At this stage it is assumed that the nominal array mechanical characteristics are accurate enough (possible deviations lower than $\lambda/10$).

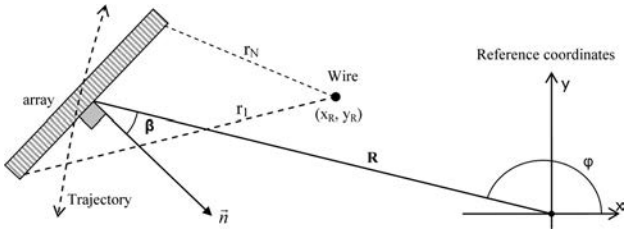

Fig. 6. Arrangement for the calibration of the array element positions.

To this purpose a single 0.1 mm copper wire normal to the array plane is put at an arbitrary position. Its unknown coordinates with regard to the absolute

reference are (x_R, y_R), assumed at the circumference centre. The distance from element i to the wire is:

$$r_i^2 = (x_i - x_R)^2 + (y_i - y_R)^2 = \left(\frac{ct_i}{2}\right)^2, \qquad (6)$$

where t_i is the measured round time-of-flight to the target and c is the sound velocity. On the other hand, the element coordinates are given by:

$$x_i = R\cos\varphi + \left(i - \frac{N-1}{2}\right) d\cos\left(\varphi - \beta - \frac{\pi}{2}\right),$$
$$y_i = R\sin\varphi + \left(i - \frac{N-1}{2}\right) d\sin\left(\varphi - \beta - \frac{\pi}{2}\right), \qquad (7)$$
$$\leq i \leq N,$$

where φ is the absolute angular position of the array centre, which is accurately known, N is the array number of elements and d is the distance between elements.

Substitution of (7) in (6) provides a set of N nonlinear equations with 4 unknowns (R, β, x_R, y_R) which can be solved by numerical methods. However, although the equation system is over-dimensioned, the measurements of the round trip time of flight are quite related to yield accurate results. But, repeating the measurements in several angular positions (changing φ) and the wire position (changing x_R, y_R) provides a larger variability on the t_i values, which yields better results for R and β. It was found experimentally that using 8 angular positions of the array (every 45°) and 4 positions of the reflector (one at every quadrant) repeatable results are obtained. By taking just the time of flight to the extreme elements, the system is composed of 64 equations with 10 unknowns and is solved by numerical methods. This procedure considers R and β constants independent of the angular position of the array. Care was taken to avoid array displacements when rotating due to, for example, the cable tension.

5. First results

Preliminary experiments were conducted to assess the performance of the proposed arrangement. Up to now, only three imaging modalities were used: phased array, image compounding and phase coherence processing. Algorithms for transmission tomography and synthetic aperture techniques are under development.

A standard medical-grade breast phantom designed to train operators for biopsies was used for the experiments (Gammex-RMI, USA). It includes reflectors and high and low scatterer density objects to mimic microcalcifications, masses and cysts. A schematic representation of the phantom at the image plane is shown in Fig. 7.

Images were obtained in the phased array mode from 36 angular positions (at 10° intervals), using the full 128-element aperture for every position. Figure 8 shows four of the phased array images (at angular positions of 0°, 80°, 140°, and 240°), which give partial views of the breast phantom.

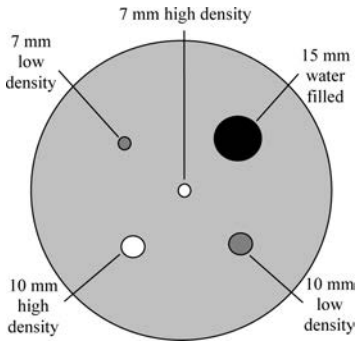

Fig. 7. Scheme of the breast phantom with high and low density scatterers' cylindrical objects.

It can be appreciated that clutter and sidelobes are rather high in the phased array imaging mode, thus, limiting the reliable detection of lesions. The diagnostics is not easy, since only a partial region of the breast phantom is seen. Finally, if taken by hand, it is difficult to reproduce any of these images.

However, when combining the 36 phased array images acquired with the circular arrangement, a full 360° view is obtained (Fig. 9). Image is shown with a 50 dB dynamic range. It can be appreciated that cysts and masses are clearly identified, as well as microcalcifications. Also, their positions are easily determined.

The resolution agrees with the theoretically expected one. Furthermore, the contrast to noise ratio (CNR) improves by image compounding, as it has been previously found by other researchers.

However, some of the reflectors that mimic microcalcifications are not well resolved over the clutter floor. Also, around the centre of the image, there are some artifacts that are due to reverberations between the "skin" and the transducer. These could be confused with tissue structures in a real examination.

Figure 10 shows a detail of the central region. At left (compounded image), the reverberation artifacts are clearly visible. Also, some of the microcalcifications show a low contrast with regard to the clutter floor level. At right, the phase coherence image of the same region is shown, where the artifacts have been suppressed and the micro-calcifications are made more evident, with a high contrast and resolution.

On the other hand, the phase coherence image alone shows a darker central region. This is due to the single focus in emission of the phased array technique, which was set halfway between the phantom centre and the perimeter in this experiment (25 mm from the center). As the emitted beam is narrow in this region, the range cell becomes thinner, which increases the scatterers coherence and hence, the phase coherence value. With synthetic aperture techniques, where emission and reception focusing is applied at all

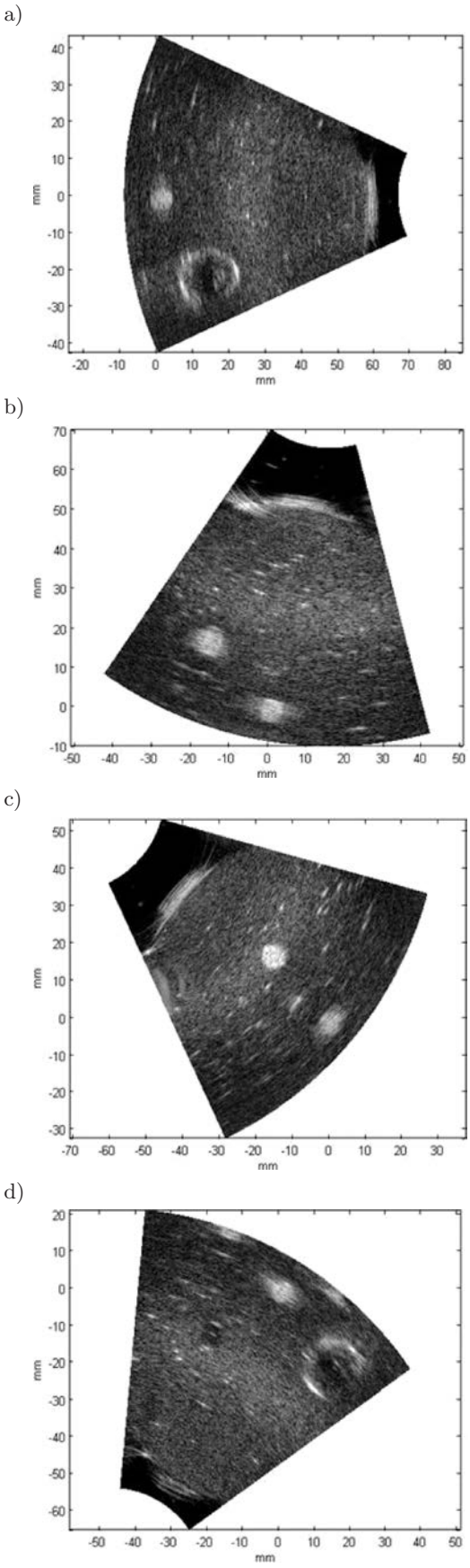

Fig. 8. Four phased array images, taken at angular positions 0°, 80°, 140°, and 240°.

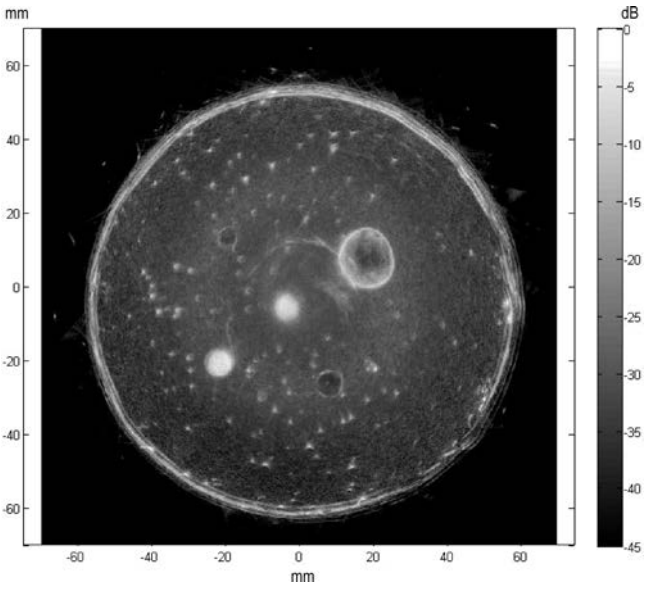

Fig. 9. Compound image of the breast phantom.

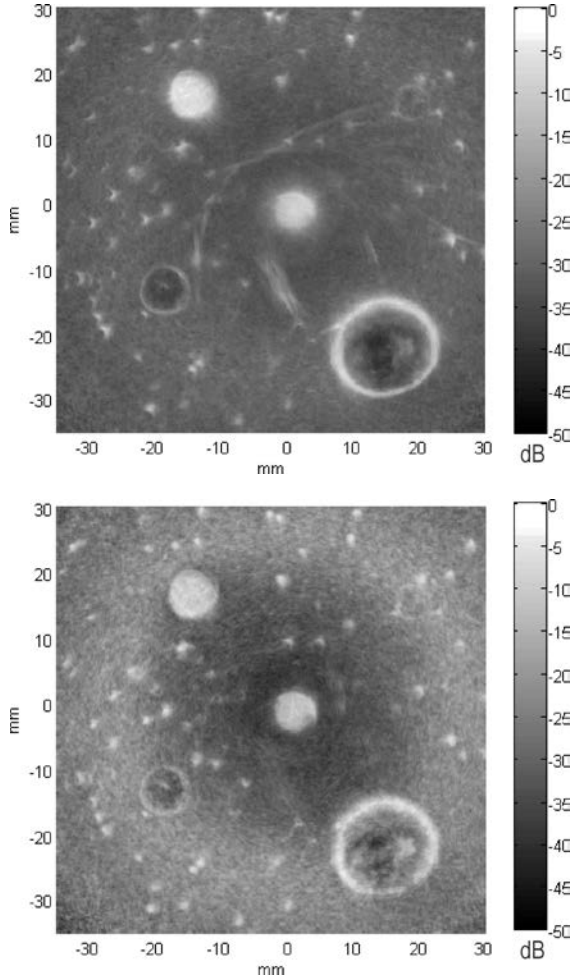

Fig. 10. Top: detail around the centre of the compound image, showing the artifacts and low-contrast to detect some micro-calcifications, bottom: phase coherence image of the same region, where the artifacts have been suppressed and the micro-calcifications get highlighted.

the imaged points, it is expected to achieve a lower clutter (better contrast) and higher resolution.

6. Conclusions

This work has been carried out to test the possibilities of ultrasound for detecting breast cancer by means of a circular geometry and multiple imaging modalities. Preliminary results with a low-cost, low frame-rate mechanical moving hardware and a standard breast phantom have been obtained using phased array, compound, and phase coherence imaging modalities. This arrangement has shown the capabilities for detecting cysts, solid masses, and micro-calcifications. A calibration procedure was required to accurately obtain the operational parameters (sound velocity in the coupling medium and position of the array elements).

It has been demonstrated that, with conventional phased array technology, slice images with reduced clutter and improved contrast-to-noise ratio are obtained by compounding many sector images taken from different angular positions. Further, phase coherence images are artifact free and provide an increased resolution and contrast. The phase coherence image information complements that of the compound image, and both can be combined by a simple multiplication.

These results indicate that a ring array surrounding a suspended breast is a good choice to improve sensitivity, resolution, and contrast for breast cancer detection. Furthermore, it provides volumetric information by taking many image slices. These images are repeatable to follow up the patient evolution after successive examinations at the prescribed periods. Also, the acquisition time for different modalities and volumetric imaging has been estimated, ranging from a few seconds to around one minute.

Acknowledgment

This work was jointly supported by the projects DPI-2010-17648 of the Spanish Ministry for Science and Innovation and S2009/DPI-1802 of the Community of Madrid. Part of this work was presented at Tecniacústica-2011 (26–28 Oct, Cáceres, Spain).

References

1. Berry D.A., Cronin K.A., Plevritis S.K., Fryback D.G., Clarke L., Zelen M., Mandelblatt J.S., Yakovlev A.Y., Habbema J.D., Feuer E.J. (2005), *Effect of screening and adjuvant therapy on mortality from breast cancer*, N. Engl. J. Med, **353**, 17, 1784–1792.
2. Camacho J., Parrilla M., Fritsch C. (2009), *Phase Coherence Imaging*, IEEE Trans. on UFFC, **56**, 5, 958–974.
3. Duric N., Littrup P., Babkin A., Chambers D., Azevedo S., Pevzner R., Tokarev M., Holsapple E., Rama O., Duncan R. (2005), *Development of ultrasound tomography for breast imaging: Technical assessment,* Med. Phys., **32**, 5, 1375–1386.
4. Duric N., Littrup P., Poulo L., Babkin A., Pevzner R., Holsapple E., Rama O., Glide C. (2007), *Detection of breast cancer with ultrasound tomography: First results with the Computed Ultrasound Risk Evaluation (CURE) prototype*, Med. Phys., **34**, 773.
5. Jensen J.A., Holm O., Jensen L.J., Bendsen H., Nikolov S.I., Tomov B.G., Munk P., Hansen M., Salomonsen K., Hansen J., Gormsen K., Pedersen H.M., Gammelmark K.L. (2005), *Ultrasound Research Scanner for Real-Time Synthetic Aperture Data Acquisition*, IEEE Trans. UFFC, **52**, 5, 881–891.
6. Jespersen S.K., Wilhjelm J.E., Sillesen H. (1998), *Ultrasound Spatial Compound Scanner for Improved Visualization in Vascular Imaging*, Proc. 1998 IEEE Ultrasonics Symposium, 1623–1626.
7. Li C., Duric N., Huang L. (2008), *Breast Imaging Using Transmission Ultrasound: Reconstructing Tissue Parameters of Sound Speed and Attenuation*, 2008 Conf. on Biomed. Engineering and Informatics, 708–712.
8. Nikolov M., Behar V. (2005), *Analysis and optimization of synthetic aperture ultrasound imaging using the effective aperture approach*, Int. J. Information Theory & Applications, 12, 257–265.
9. Nothacker M., Duda V., Hahn M., Warm M., Degenhardt F., Madjar H., Weinbrenner S., Albert U.S. (2009), *Early detection of breast cancer: benefits and risks of supplemental breast ultrasound in asymptomatic women with mammographically dense breast tissue*, BMC Cancer, **9**, 335,
10. Quan Y., Huang L. (2007), *Sound-speed tomography using first-arrival transmission ultrasound for a ring array*, Proc. SPIE Medical Imaging, 6513, 651306-1-9.
11. Romero D., Martinez–Graullera O., Martin C.J., Higuti R.T., Octavio A. (2009), *Using GPUS for beamforming acceleration on SAFT imaging*, Proc. IEEE Ultrason. Symp., 1334–1337
12. Stozka R., Widmann H., Müller T.O. (2004), *Prototype of a new 3D ultrasound computer tomography system: transducer design and data recording*, Med. Imag, 5373, 70–79.
13. Szabo T.L. (2004), *Diagnostic ultrasound imaging*, Elsevier Academic Press.
14. Teh W., Wilson A.R.M. (1998), *The role of ultrasound in breast cancer screening. A Consensus Statement by the European Group for Breast Cancer Screening*, European Journal of Cancer, **34**, 4, 449–450.
15. Trots I., Nowicki A., Lewandowski M., Tasinkevych Y. (2010), *Multi-Element Synthetic Transmit Aperture in Medical Ultrasound Imaging*, Archives of Acoustics, **35**, 4, 687–699.
16. Waag R.C., Fedewa R.J. (2006), *A Ring Transducer System for Medical Ultrasound Research*, IEEE Trans. on UFFC, **56**, 5, 958–974.